Fixed-node diffusion Monte Carlo method for lithium systems

K. M. Rasch* and L. Mitas†

Department of Physics, North Carolina State University, Raleigh, North Carolina 27695, USA

(Received 25 February 2015; revised manuscript received 29 June 2015; published 24 July 2015)

We study lithium systems over a range of a number of atoms, specifically atomic anion, dimer, metallic cluster, and body-centered-cubic crystal, using the fixed-node diffusion Monte Carlo method. The focus is on analysis of the fixed-node errors of each system, and for that purpose we test several orbital sets in order to provide the most accurate nodal hypersurfaces. The calculations include both core and valence electrons in order to avoid any possible impact by pseudopotentials. To quantify the fixed-node errors, we compare our results to other highly accurate calculations, and wherever available, to experimental observations. The results for these Li systems show that the fixed-node diffusion Monte Carlo method achieves accurate total energies, recovers 96–99 % of the correlation energy, and estimates binding energies with errors bounded by 0.1 eV/at.

DOI: 10.1103/PhysRevB.92.045122 PACS number(s): 02.70.Ss, 31.15.V−, 71.10.−w, 71.15.−m

I. INTRODUCTION

Quantum Monte Carlo (QMC) methods have been applied to a great variety of electronic structure problems over the past three decades. These calculations provide a number of highly accurate results for properties such as cohesion and binding energies, excitations, reaction barrier heights, defect formation energies, and other quantities; they are typically in excellent agreement with available experiments [1,2]. In addition, the calculations have shed new light on correlation effects in various systems, and therefore they have become valuable as benchmarks for other methods and comparisons. The most important strength of this approach is that the many-body Hamiltonian is employed directly, and thus the electron-electron interaction and particle correlations are treated explicitly in a many-body manner. Another advantage of QMC methods is its ready applicability to large systems of interacting particles so that properties of solids can be calculated by using supercells and extrapolations to the thermodynamic limit.

The diffusion Monte Carlo (DMC) method projects out the ground state of a system by applying the projection operator $\exp(-\tau H)$, where H is the Hamiltonian, to the trial wave function Ψ_T. While any Hamiltonian can be evaluated, we discuss electron systems with the fully interacting Coulomb potential. In the large imaginary-time limit $\tau \to \infty$, the ground state of a given symmetry is obtained. One of the fundamental limitations in achieving exact results is the so-called fixed-node (FN) approximation, which enables one to avoid the well-known fermion sign problem [1,3]. The fixed-node approximation is difficult to improve upon since the corresponding energies are typically very small, e.g., a few percent of the correlation energy, where the correlation energy is itself a small fraction of the total energy. Therefore, systematic improvements of the nodes through minimization of the total energy or variance of the energy for a given trial wave function is laborious and often very costly [4,5]. Insights into the role of basis sets in the error [5] were not always easy to utilize in different systems [6]. Improvements in algorithmic efficiency, in the speed and quality of wave-function optimization routines, and in functional forms for orbitals and wave functions continue, and yet a significant amount of work remains to be done in simply understanding the root origin of the nodal errors by systematically quantifying the dependence of energy biases on the nodal defects.

Recently, we have analyzed the impact of the electron density on the nodal bias in a set of free-atom/ion systems, and we found the fixed-node errors to be proportional to the density in this particular class of systems for both the spin-unpolarized [7] and spin-polarized [8] cases. A similar pattern of increasing fixed-node errors with larger charge density in the region of nodal errors was observed in the presence of pseudopotentials [9]. As a testbed to expand this study to more complicated cases, a series of lithium systems is attractive for several reasons. First, inclusion of the core electrons in Li calculations is computationally feasible. That enables us to avoid any additional, more complicated analysis that is necessary whenever pseudopotentials or effective core potentials are being employed. This ensures that any missing amount of the binding energy, cohesive energy, or correlation energy is caused solely by the fixed-node approximation. Second, the exact wave function for a free Li atom has a relatively simple nodal surface that is already well approximated at the Hartree-Fock level. In addition, small Li systems have been studied with the FN-DMC method before. In this work, we significantly expand upon previous studies with calculations of Li_4 clusters and Li solid in its equilibrium body-centered-cubic structure. By comparing our fixed-node diffusion Monte Carlo (FN-DMC) results with other accurate calculations and experimental results corrected for zero-point motion (DMC is carried out in the Born-Oppenheimer approximation), we can assess the magnitude of the fixed-node errors with high accuracy. These systems represent a variety of environments for the bonding and include directional bonds, multicenter bonds, and delocalized metallic bonds. It is therefore an interesting question to understand how the fixed-node bias changes once Li enters bonding in the setting of molecular bonds or periodic boundary conditions. Based on these results, we establish a systematic picture of the nodal errors in Li systems and corresponding accuracies for energy differences.

*kmrasch@ncsu.edu
†lmitas@ncsu.edu

II. METHODS

In DMC, we solve for the ground-state solution of Schrödinger's equation,

$$\Psi_0 = \lim_{\tau\to\infty} \exp\{-\tau\mathscr{H}\}\Psi_T, \quad (1)$$

where $\mathscr{H}$ is the Born-Oppenheimer Hamiltonian. The antisymmetric nature of fermion systems poses a challenge to the naive application of the DMC algorithm and leads to the fermion sign problem [3,10,11]. This is because for a given boundary value problem, the eigenstate with the lowest eigenvalue will be a symmetric state. In light of this well-known difficulty, perhaps the simplest and most straightforward way to circumvent the sign problem is the fixed-node approximation.

Under the fixed-node approximation, we impose a boundary condition at the nodes of the trial wave function and maintain them for the duration of the simulation. The nodes form a hypersurface defined implicitly by

$$\Omega = \{\mathbf{R}; \Psi_T(\mathbf{R}) = 0\}. \quad (2)$$

The assumed nodal hypersurface creates boundaries that constrain the solution in each nodal cell and preserve the overall fermionic antisymmetry of the total wave function, thus preventing any appearance of "signs." This allows one to ignore the sign of the wave function inside the nodal cell and to carry out the DMC algorithm within each nodal cell,

$$\Psi_T\Psi_0 \geqslant 0. \quad (3)$$

Unfortunately, doing this exactly is a tall order. It requires that for an N-electron system, one must have a description of the exact $(3N-1)$-dimensional hypersurface Ω. Solving for such a hypersurface directly is beyond our means, and instead we proceed by using nodal surfaces from approximate wave functions. Because we use a nodal hypersurface that is not exact, the solution will have a higher energy than the exact ground state, i.e., the total energy computed via FN-DMC is a variational upper bound to the exact energy [12]. Further details on the FN-DMC method can be found elsewhere; see, for example, Ref. [1].

The trial functions used in this study are of the Slater-Jastrow type,

$$\Psi_T(\mathbf{R}) = \sum_k c_k \det{}_k^{\uparrow}[\varphi_i]\det{}_k^{\downarrow}[\varphi_j]\exp(U), \quad (4)$$

where the one-particle orbitals are obtained from Hartree-Fock (HF) or density-functional theory (DFT). More details on the trial functions and their optimizations, Jastrow correlation factors, and DMC calculations for periodic boundary conditions can be found in the recent review in Ref. [2]. We used the QWALK software package to carry out all QMC calculations [13].

III. RESULTS

A. Lithium atom and electron affinity

To calculate the total energy of the lithium atom, we use a restricted Hartree-Fock wave function. Since the spin-up and spin-down subspaces are independent at the HF level, the minority spin channel contains only one electron, and the wave function's node exists in only the spin majority subspace. We can visualize this subspace of the nodal hypersurface by considering the wave function when 1 and 2 label the electrons in the same spin channel. Then it follows from the form of the HF determinant that the node is given by the condition $r_1 = r_2$. The electron labeled as 1 therefore "sees" the node as a sphere that passes through the position of electron 2 and has the nucleus as its origin. The wave function will be equal to zero if electron 1 occupies any point on the spherical nodal surface.

TABLE I. Comparison of theoretical results for the total energy of a lithium atom where FN-DMC energy has been obtained with the HF nodes.

Source	Total energy (Ha)
HF	−7.23641
FN-DMC present work	−7.47801(1)
FN-DMC Bressanini *et al.* [15]	−7.478060(3)
exact [16]	−7.47806032

The exact HF nodal hypersurface in the full 6D space is a 5D hyperboloid given by the implicit equation $x_1^2 + y_1^2 + z_1^2 = x_2^2 + y_2^2 + z_2^2$. As pointed out by Stillinger *et al.* [14], this is not strictly exact, as the correlation with the electron in the spin-down channel will cause deformations away from a perfect sphere. For example, the excitation $2s^1 2p^2$ will have a contribution to the exact ground state and would in principle lead to a departure from the single-particle node (i.e., the sphere will deform slightly to an ellipsoid or perhaps a more complicated surface that would depend on the position of the minority spin electron). It is therefore quite remarkable that the HF nodal surface seems to be so accurate: the total energy with the HF nodes, shown in Table I, is accurate to ≈0.05(1) mHa, and the fixed-node bias is less than 0.1% of the correlation energy [15]. This demonstrates that the correlation is basically completely captured by the Jastrow-like effect, and it affects the 5D hyperboloid only marginally. (This contrasts with the Be atoms where the nodal surface is strongly affected by correlations [7].)

Our own calculated fixed-node error in the single atom energy is ≈0.05(1) mHa, much smaller than the chemical accuracy (≈1.6 mHa). This also suggests that any fixed-node errors in the aggregate species from Li atoms will be essentially identical to the error in the binding or cohesive energy.

We can compute the electron affinity of a Li atom using the value for the ground-state total energy of the Li^- ion from Ref. [7], which has a fixed-node error comparable to the neutral atom. The electron affinity is given by

$$\mathrm{EA(Li)} = E_0(\mathrm{Li}) - E_0(\mathrm{Li}^-). \quad (5)$$

Lithium has a positive electron affinity, meaning the anion is more stable than the neutral atom. The HF limit of the total energy of Li^- has been computed to be −7.428 232 0 Ha; the HF limit of the total energy of the neutral Li atom is −7.432 726 93 so that in the HF approximation the additional electron would not be energetically favorable [17–19]. As is well known, correlation effects are crucial for describing the electron affinity with accuracy comparable to experiment [19].

TABLE II. Comparison of the latest calculation and measurement with FN-DMC results for the electron affinity for Li (in Ha).

Author	Method	EA (Ha)
Fischer [21]	extrap. MCHF	0.022698
Present work	FN-DMC HF single det.	0.0201(1)
Present work	FN-DMC 2 configs.	0.02279(5)
Haeffler [20]	Expt.	0.0227129(8)

Using a wave function composed of two configuration state functions, i.e., the HF reference state plus $2s^2 \rightarrow 2p^2$ excitation (a symmetry-adapted linear combination of determinants), for the four-electron ion yields an FN-DMC electron affinity with an excellent accuracy compared to experimental measurement [20]. The best theoretical and experimental data are compared with this work in Table II. While the two species in the calculation share geometric details (the central potential in free space), when the fourth electron is added the nodal hypersurface changes and the anion shows a nodal shape similar to the isoelectronic Be atom. The poor quality of the result for the electron affinity using only a single determinant trial function for Li^- stands to illustrate that the extreme accuracy of the RHF nodal hypersurface for three electrons is not typical and is rather a result of a fortuitous coincidence.

B. Li_2

The Li_2 dimer is a more complicated system. The additional Li atom increases the number of electrons and changes in the overall real-space geometry from one central potential with spherical symmetry to a two-potential cylindrical symmetry. The nodes of the lithium dimer have been studied a number of times [22,23]. The best single configuration result in the literature (in Ref. [23]), $E_{\text{FN-DMC}} = -14.9923(1)$, has about 3.1 mHa fixed-node error. The fixed-node error of the best wave function in the same reference is ≈0.2–0.3 mHa, with a total energy of −14.9952(1). Using the value for the HF energy reported by Filippi and Umrigar [22], this recovers ≈99.8% of the correlation energy. Bressanini *et al.* [23] have pointed out that a five-configuration wave function has the nodal surface close to the exact one, and therefore it is not too difficult to obtain accurate energies at the fixed-node approximation level with errors of the order of 0.1% as well. Interestingly, only the three lowest excitations were really involved: $2\sigma^2 \rightarrow 1\pi^2$, $2\sigma_g^2 \rightarrow 2\sigma_u^2$, and $2\sigma_g^2 \rightarrow 3\sigma_g^2$. Since this system was studied exhaustively, we did not repeat the multireference calculation, and instead we quote the results of Bressanini *et al.* [23] hereafter.

C. Li_4

Li_4 and its properties have been studied by several methods, including the basis-set correlated approaches [24–29]. The most stable configuration of four Li atoms is a molecule with D_{2h} symmetry, a planar rhombus geometry, and a singlet electronic ground state [24–28]. The geometry of the D_{2h} Li_4 is depicted schematically in Fig. 1. This can be understood as the result of a Jahn-Teller distortion of the more symmetric geometry of a square [26]. Li_4 exhibits a "three-center"

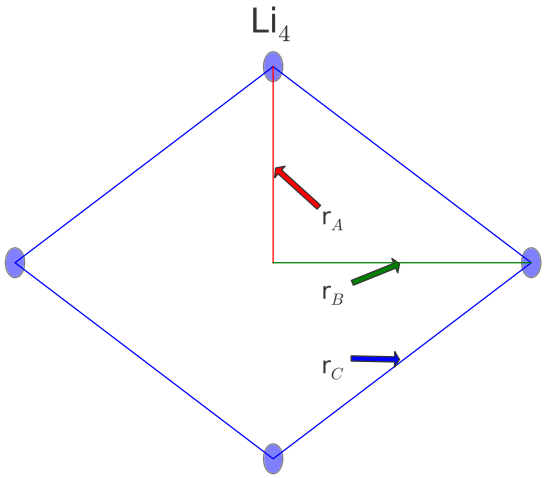

FIG. 1. (Color online) Schematic depiction of the D_{2h} Li_4 parameters.

bonding pattern where two electrons are shared inside each of the two triangles formed by bisecting Fig. 1 along the "r_A" line [30].

In Table III, we compare the nodes of the SCF wave functions (unoptimized) for different levels of CI in order to illustrate the behavior of such expansions and to select the best starting place for our QMC trial wave function. For each level of CI, we used complete expansions but limited the number of virtual orbitals in the active space. It is clear that the nodes do not improve systematically for larger active space and a higher level of theory as the CI total energies do.

Since FN-DMC errors associated with the basis set are not very systematic, we also tested the nodal surfaces of several basis sets to minimize these errors. Although not fully complete, the results seem to support the conclusion of Bressanini *et al.* [23] that for Li systems, saturating the *s* channel is more important than adding additional high angular momentum basis functions. These results are listed in Table IV. After some initial testing of basis and multideterminant expansions, we employed wave functions constructed from the aug-cc-pCVTZ basis and included the 15 lowest-lying virtual orbitals into the CI-SD calculation. We reoptimized the weights of the resulting 93 configuration-state functions in the CI expansion with VMC total energy minimization using a Levenberg-Marquardt algorithm. The geometry parameters

TABLE III. Fixed-node DMC total energies (a.u.) for trial wave functions from different levels of CI. These calculations were used to test unoptimized nodal surfaces for use as DMC trial wave functions. The corresponding CI energies are included as well.

Theory	Virtual orbitals	E_{CI}	$E_{\text{FN-DMC}}$
RHF	0	−29.76238	−30.0177(5)
CI-SD	9	−29.81584	−30.0184(5)
CI-SDTQ	9	−29.82021	−30.0174(4)
CI-SD	15	−29.82475	−30.0228(4)
CI-SDTQ	15	−29.83131	−30.0179(4)
CI-SD	19	−29.82534	−30.0162(4)
CI-SDTQ	19	−29.83226	−30.0179(6)

TABLE IV. FN-DMC results for different basis sets with trial wave functions from CI-SD calculations using 15 virtual orbitals and then optimized in with respect to VMC total energy.

Basis set	Total energy (Ha)
Roos Aug. DZ ANO ($4s3p2d$)	−30.02127(5)
Roos Aug. TZ ANO ($4s4p3d2f$)	−30.02119(6)
aug-cc-pCVTZ ($7s6p4d2f$)	−30.02263(6)

have been computed a number of times in the literature, as reported in Table V, organized by the value for the Li-Li distance labeled r_C in Fig. 1. The FN-DMC results indicate that there is a short Li-Li bond ≈2.64 Å ($2r_A$ in Fig. 1) and a longer Li-Li bond ≈2.99–3.0 Å (r_C in Fig. 1).

The experimental and theoretical binding energies of Li_4 are given in Table VI. Because the presence of the Jastrow factor will influence the optimization of the multideterminant expansion, it is not clear *a priori* what form of the Jastrow factor is optimal. In particular, since the bonds are not very strong and the bond lengths are somewhat larger than in typical single-bonded situations, we tested the range of the Jastrow cutoff distance parameter. We optimized the Jastrow coefficients and determinant weights for two different electron-ion Jastrow distances. The wave function with the so-called "short-range" Jastrow effects had its electron-ion and electron-electron-ion terms extend to 2.45 bohr from each atom, i.e., to just less than half the smallest Li-Li distance. For the "long-range" Jastrow, the electron-ion terms were allowed to extend to 7.5 bohr. The qualitative difference between these two Jastrows is that terms from different atoms in the short-range Jastrow do not overlap in the region occupied by the three-center bonds. This difference in description of the wave function translates into a difference in computational effort. In the "short-range" case, each electron will have nonzero three-body Jastrow terms associated with only one atomic center at any given time, whereas in the "long-range" case, electrons have nonzero contributions to the Jastrow coming from each of the Li atoms surrounding the three-center bonding region. The resulting effect in the total energy of the wave function was only ≈0.000 13 per atom.

We carried out a time-step extrapolation for both wave functions, shown in Fig. 2, to ensure that the time-step error is $<$ ≈0.05 mHa in the total energy, or an order of magnitude smaller than the statistical error bars in the binding energy. After correcting for the zero-point motion, which is about 3.12 mhartree per atom [28], we find a binding energy of 0.723(3) eV. Note the reasonably good agreement between the results, although the basis-set correlation methods did not include any correlation of the core ($1s$) states. This points out that the core states are already quite deep and do not affect the nodal surfaces significantly. One of the reasons is that any excitation that would correlate the $1s$ level would involve states that would lie very high in energy since such excitations would require a strongly localized type of orbitals. The accuracy of these results and those presented for the Li dimer suggest that the nodal surfaces are minimally affected by the $1s$ subshell.

TABLE VI. Binding energies of Li_4, uncorrected for zero-point motion, are given in units of eV per atom.

Author	Method	Binding
Alikhani and Shaik [32]	DFT	0.61
Bonacic-Koutecky *et al.* [33]	MRD-CI	0.63
Owen [34]	DMC	0.67(2)
Nissenbaum *et al.* [29]	DMC	0.733(4)
Rao *et al.* [35]	CI-SD	0.7375
Wheeler *et al.* [28]	CCSD(T)	0.7445
Present work	DMC	0.744(3)
Wu [36]	Expt.	0.84(5)
Brechignac *et al.* [37]	Expt.	0.63(4)

The table includes also experimental data from the two available sources, namely Wu [36] and Brechignac *et al.* [37] [0.84(5) and 0.63(4) eV, respectively]. These data show significant differences and seem inconsistent with each other. Considering the reasonable agreement between the four independent calculations in Table VI that are within ≈0.01 eV and the sizable error bars on the experimental values, we essentially claim that our present calculation, being produced by an upper bound method and having the lowest total energy of the theoretical calculations, is the most accurate estimation of this total energy to date.

D. Bulk lithium in a bcc crystal

Because of its position as a bulk crystal with only one valence electron per atom, lithium in the body-centered-cubic (bcc) crystal (Pearson symbol cI2) has been studied a few times by QMC methods in the literature [38–41]. Surprisingly, however, none of these calculations has used FN-DMC with the core electrons included.

Further interest in studying lithium crystals with QMC methods was stimulated by recent experimental and theoretical developments. For example, interesting phenomena for high pressures, including superconductivity, have been reported in experimental studies [42,43]. An intriguing hypothetical suggestion has been raised by Neaton and Ashcroft that lithium solid may undergo a Peierls transition into a so-called

TABLE V. Summary of the optimized geometry parameters of D_{2h} Li_4 tested in this work, and the FN-DMC total energy for each. The trial wave function is an VMC energy-optimized CI-SD expansion with 93 CSFs.

Author	Method	r_A (Å)	r_B (Å)	r_C (Å)	$E_{\text{tot}}^{\text{FN-DMC}}$ (Ha)
Ray [24]	DFT	1.298	2.759	3.050	−30.02132(2)
Rousseau and Marx [27]	QCISD/CCSD(T)	1.323	2.700	3.007	−30.02155(2)
Verdicchio *et al.* [31]	CCSD(T)	1.323	2.680	2.989	−30.02158(2)
Wheeler *et al.* [28]	CCSD(T)	1.316	2.681	2.987	−30.02154(2)

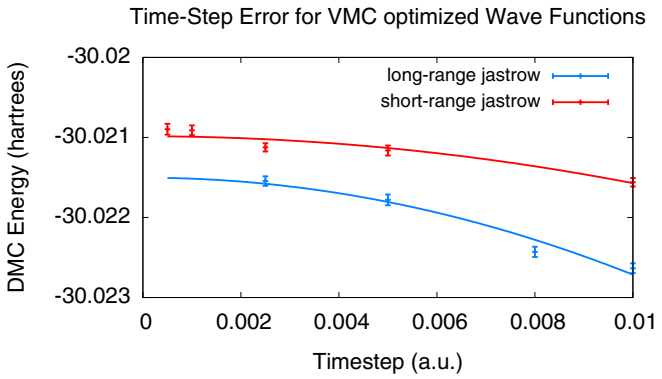

FIG. 2. (Color online) The DMC energy extrapolated to $\tau = 0$ for a Li_4 molecule. Both wave functions originate from the same configuration-interaction CI-SD calculation, but they have had the determinant weights and Jastrow coefficients reoptimized with different assumed cutoff distances in the Jastrow, as described in the text.

"alkali electride" at high pressures, an exotic phase in which paired Li atoms are stabilized by pockets of highly localized electrons [44,45].

Experimental measurements of the lattice constant of bcc lithium agree that $a_0 = 3.51$ Å (Refs. [46–51]). Previous QMC simulations treat 3.482 Å (given as 6.58 bohr) or similar values as the experimental value, perhaps due to the fact that the experimental measures were done at 25 °C (Refs. [38–41]). Gaudoin and Foulkes suggest that for zero-temperature methods, the computed equilibrium is expected to be $a_0 = 3.44$ Å (Ref. [52]). While we did not construct a full energy-volume curve, we checked these lattice constants with both DFT and FN-DMC, shown in Table VII. At the DFT level, the difference at the extremes of these lattice values is ≈1.5 mHa. The difference at the FN-DMC is smaller, ≈0.25 mHa, and since the finite-size errors are still present in these values, this likely overshadows the actual differences between the lattices.

We consider the differences between different lattice constants to be rather small, and for the sake of consistency with previous QMC calculations we further study the cI2 lithium solid by FN-DMC at the lattice constant $a_0 = 3.482$ Å. Our FN-DMC calculations use a single determinant Slater-Jastrow wave function with orbitals taken from DFT calculations. Since the nodal surface would be rather difficult to improve upon within the QMC calculation of a crystalline system, we begin by comparing several DFT functionals to find the best nodal surface, and we found the results to lie within 2–2.5 mHa per atom of the highest quality

TABLE VII. Total energy per atom in atomic units from DFT/PBE-PZ and FN-DMC calculations for a 16-atom cell (2 × 2 × 2 conventional cell) for different lattice values.

a_0 (Å)	DFT	FN-DMC
3.51	−7.60873	−7.53840(3)
3.482	−7.60914	−7.53852(2)
3.44	−7.61027	−7.53867(2)

TABLE VIII. Results of FN-DMC calculations for the Γ-point wave function of an eight-atom supercell comparing the nodal quality of orbital sets generated by DFT functionals.

Exchange	Correlation	E_{tot} (hartrees)
H-F		−60.135(1)
PW91-GGA	PW91-GGA	−60.136(1)
PBE-GGA	PBE-GGA	−60.144(1)
PBE-GGA	PZ-LDA	−60.151(1)

nodal surface (PBE-PZ functional). This strategy has been motivated by our work on DFT generated orbital sets to find the most optimal nodal surface [53,54]. A select subset of the functionals tested are reported in Table VIII. The total energy is integrated over the irreducible Brillouin zone by the so-called "twist-averaging" procedure: a DMC calculation is carried out for each symmetry-unique k-point in a uniform $8 \times 8 \times 8$ Monkhorst-Pack mesh, and the resulting energies are weight-averaged using the geometric multiplicity of the k point as the weight [55]. To treat the finite-size errors that occur, both due to the Ewald sums and also to the finite number of twists, we collect statistics on the static structure factor $S(k)$ during the QMC simulations. These data are plotted in Fig. 3. The correction to the finite-size errors in the simulation cell's energy is calculated using the functional form for $S(k)$ as detailed by Chiesa *et al.* [56]. The 8-atom (triangle symbols) and 16-atom (circle symbols) data for variational Monte Carlo (VMC) and DMC mixed estimators are less well converged when compared to the 54-atom cell. The corrected DMC mixed estimator (blue) is, however, consistent for all sizes of cell. This suggests that, at least for some systems, it is possible to estimate the static structure factor correction accurately with data from smaller simulation cells. Since the system is a simple metal, within the random-phase approximation the behavior

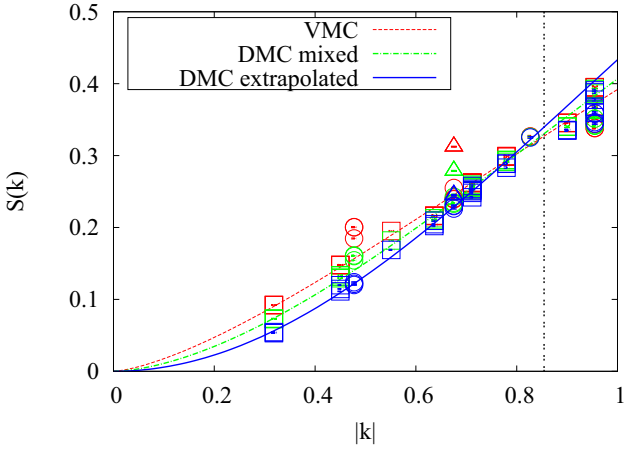

FIG. 3. (Color online) QMC results for $S(k)$ for several sizes of the simulation cell. Squares denote results from the 54-atom simulation; circles, 16-atom simulation; and triangles, eight-atom simulation. The curves shown are fit to the 54-atom data with the function $S(k) = \exp\{-ak^b\}$. For small k, RPA predicts $b = 2$. For the fits shown, the b parameter for VMC is 1.45; DMC with the mixed estimator, 1.67; and the DMC extrapolated estimator, 1.99.

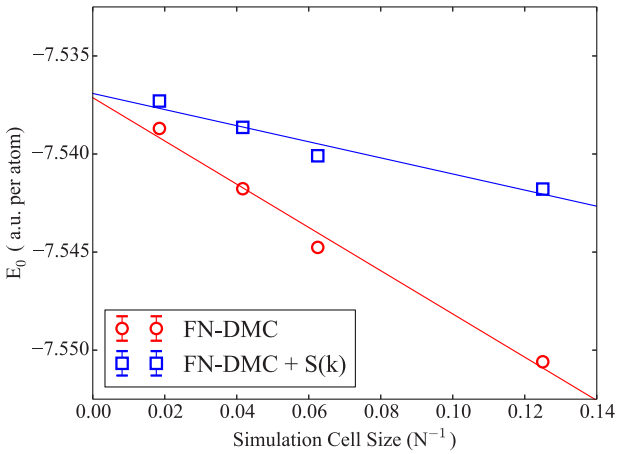

FIG. 4. (Color online) The total energy per atom for twist averaged FN-DMC with and without the finite-size error (FSE) corrections [56] plotted against the inverse of the number of atoms in the cell. The data are fit with an extrapolation to infinite bulk size. The infinite bulk total energy per atom of −7.5371 Ha for the FN-DMC and −7.5369 for the FN-DMC with FSE corrections. These values are within error bars of each other. The statistical error bars on the data are smaller than the size of the plot symbol, thus they are not visible.

of $S(k)$ for small values of k is expected to be proportional to k^2, as detailed by Bohm and Pines [57]. The curve fit to our calculated values indicates that $S(k)$ in our simulation is $\propto k^{1.99}$ so that we have reasonable confidence in the quality of the corrected mixed DMC estimator result [1]. We use a linear fit to the equation

$$E_n = E_\infty - \frac{a}{N} \tag{6}$$

to extrapolate the total energy per atom to the infinite bulk of the cI2 lithium crystal, as shown in Fig. 4. The data in Fig. 4 show that after applying twist averaging and corrections, the 16-atom cell energy per atom is ≈2.5 mHa from the infinite bulk value, and the 24-atom cell is ≈1 mHa, while the 54-atom cell is less than a mHa from the extrapolated value. We believe that the Li bulk energy could be further improved by more sophisticated orbitals and optimization by employing more accurate wave functions, such as the ones based on pair orbitals [29,58,59]; however, in this study the focus was to understand the trial functions that are, at present, commonly used for solid-state and quantum chemistry calculations.

E. Discussion

To compare the quality of the results for these systems, Table IX shows the per atom energy evolving toward the bulk value as the size of the lithium system increases. These values are based either on the best total energy calculations available or on using experimental binding and estimated zero-point motion energies subtracted from the exact atomic energy. Therefore, they represent the depths of the binding curves assuming $T = 0$ and infinite nuclear masses, similar to previous studies; see, for example, Ref. [22]. For the lithium dimer, we quote the values of Ref. [23]. For the Li_4 cluster, we list our own FN-DMC calculated binding energy on the

TABLE IX. Summary of the estimated total energies per atom for a sequence of different sized Li systems. E_0 for the $n = 4$ cluster we substitute use the obtained FN-DMC value for the binding energy.

Size	$E_{\text{FN-DMC}}$	Est. E_0	Estimated from
1	−7.4780(1)	−7.47806	Hylleraas expan.
2	−7.4976(1)[a]	−7.4977	Expt.+ZPM[b]
4	−7.50538(1)	−7.50541	FN-DMC binding
cI2 crystal	−7.5369(6)	−7.54066	Expt.+ZPM[c]

[a]From Ref. [23].
[b]Atom + ZPM+ experimental binding from Ref. [22].
[c]Atom + ZPM + experimental binding from Refs. [60,61].

grounds that it is the best currently available estimation. For the body-centered-cubic crystal, we take an estimate of the zero-point vibrational energy of 0.001 72 Ha from Ref. [60], and the cohesive energy of 0.060 87 Ha from Ref. [61], and we subtract these from the exact single-atom total energy. The quoted value of the experimental cohesive energy is obtained from the enthalpy extrapolated to $T = 0$ using experimental data; see Refs. [61,62]. Table IX shows the per atom energy evolving toward the bulk value as the size of the lithium system increases.

The imperfect result for the FN-DMC correlation energy of the Li solid is still very accurate, higher only by the fixed-node bias of about 3.7 mHa (≈4% of the correlation energy) from the estimated exact value. The underestimation of the cohesive energy is essentially the same, approximately 0.1 eV. We consider this to be remarkably accurate in light of the simplicity of the single-reference Hartree-Fock wave-function nodes. Given the fact that the spin-up and spin-down channels are completely decoupled in HF, the complexity of the nodal surface is not fully captured by this trial function; nevertheless, the accuracy of the total energy appears to be quite robust so that the impact of these errors is comparably small. We conjecture that the electronic structure is dominated by the nearly-free-electron picture that is far from the strongly correlated regime. Therefore, the single-reference wave functions lead to qualitatively and also quantitatively accurate descriptions of the ground-state properties of the Li solid.

Taking the analysis of the Li crystal further, we can divide the bias into essentially two components, namely one that has the atomic (core-valence) origin and the remaining "homogeneous" (valence-valence) part. These two components result from imperfections in capturing core-valence correlations and valence-valence correlations of the metallic $2s$ band. Qualitatively, the order of magnitude of the atomic part can be extracted from the Li_2 molecule as well as from the Li^- anion. Note that in Li_2 (Li^-), one-particle states can be partitioned into the core singlets $1s^2$ and the valence singlet $2\sigma_g^2$ ($2s^2$). The separated cores are essentially nodeless, and the separated valence singlet is nominally nodeless as well (note that the one-particle nodes are generated by the orbital orthogonality and they do not correspond to the many-body fermion nodes). The fermion nodes are formed by antisymmetrization between the core and valence electrons, i.e., they belong to the core-valence subspace of correlations. Considering Li_2 as a good model for these types of correlations, the fixed-node error in the molecule for the single-reference Slater-Jastrow trial

function is about 0.0032 Ha in total, and therefore ≈0.0016 Ha per Li atom. Similarly, for the Li^- anion the corresponding value is about 0.0026 Ha. Therefore, we consider ≈0.002 Ha per atom as a reasonable estimation for the core-valence fixed-node bias. Besides this core-valence component, the remaining correlations of the Li crystal are in the valence-valence subspace of the 2*s* metallic band. Away from the core regions, these metallic states are smooth, delocalized, and form a system that is close to the homogeneous electron gas (HEG), a well-known paradigmatic model for a metal. The valence electronic density of our simulation cell corresponds to the Wigner-Seitz radius $r_s \approx 3.24$, and therefore we can estimate the order of magnitude of the fixed-node error of the Slater-Jastrow wave function in HEG using previous studies. Accurate values of the HEG energies and the corresponding Slater-Jastrow fixed-node errors are known for some values of r_s based on nearly exact calculations with backflow wave functions; for further details, see Refs. [59,63–66]. Using these results, the estimated fixed-node error is about 0.0013 a.u. (small differences between the studies are not crucial for our purposes here). Interestingly, we see that the nodal error contributions from the atomic inhomogeneities (core-valence) and from the homogeneous metallic band are of comparable sizes. It is reassuring that the sum of these two components is ≈0.0035 a.u., which is very close to the fixed-node error we found. This finding also suggests the barrier to eliminating the remaining fixed-node bias. Clearly, one would need to address both the localized (core-valence) correlations as well as the HEG-like (valence-valence) correlations on the same footing. In the future, perhaps an expansion in local atomic excitations can be combined with backflow terms so that the resulting trial wave function would capture both components of the overall missing correlations.

IV. CONCLUSION

As the size of Li systems increases from a single atom to the bulk crystal, it is clear that the complexity of the nodal hypersurface grows. In the simplest case of the atom, a nearly exact approximation to the node is known. For related small systems, the nodal errors are small, and it is possible to recover almost exact nodes with acceptable sizes of expansions in excited determinants. What is valuable and somewhat unexpected is the fact that the accuracy of the FN-DMC calculation with single reference trial functions is high even for the Li solid. Note that the solid phase is metallic, so that its electronic structure is different from atomic and molecular systems with localized ground states. The presented calculations show that for Li systems, readily available trial wave functions are sufficiently accurate to provide cohesive and binding energies to within an accuracy of 0.05–0.1 eV. We also find that the remaining fixed-node error in the Li solid for the Slater-Jastrow wave function is almost equally divided between the core-valence and the valence-valence contributions. Our understanding of the fixed-node errors is gradually advancing, and the results presented here add another piece into the mosaic of previously obtained insights that indicate that both the electronic density and the complexity of bonds, particularly the bond multiplicities, strongly influence the nodal accuracy.

ACKNOWLEDGMENTS

This research was supported by the U.S. Department of Energy (DOE), Office of Science, Basic Energy Sciences (BES) under Award No. DE-SN20084 (SC0012314). We would also like to thank Jindřich Kolorenč for insightful discussions in the early stages of these calculations.

[1] W. M. C. Foulkes, L. Mitas, R. J. Needs, and G. Rajagopal, Quantum Monte Carlo simulations of solids, Rev. Mod. Phys. **73**, 33 (2001).

[2] J. Kolorenc and L. Mitas, Applications of quantum Monte Carlo methods in condensed systems, Rep. Prog. Phys. **74**, 026502 (2011).

[3] P. J. Reynolds, D. M. Ceperley, B. J. Alder, and W. A. Lester, Fixed node quantum Monte Carlo for molecules, J. Chem. Phys. **77**, 5593 (1982).

[4] F. A. Reboredo, R. Q. Hood, and P. R. C. Kent, Self-healing diffusion quantum Monte Carlo algorithms: Direct reduction of the fermion sign error in electronic structure calculations, Phys. Rev. B **79**, 195117 (2009).

[5] C. J. Umrigar and C. Filippi, Energy and variance optimization of many-body wave functions, Phys. Rev. Lett. **94**, 150201 (2005).

[6] L. Bertini, M. Mella, D. Bressanini, and G. Morosi, Borromean binding in H_2 with Yukawa potential: A nonadiabatic quantum Monte Carlo study, Phys. Rev. A **69**, 042504 (2004).

[7] K. M. Rasch and L. Mitas, Impact of electron density on the fixed-node errors in quantum Monte Carlo of atomic systems, Chem. Phys. Lett. **528**, 59 (2012).

[8] A. Kulahlioglu, K. M. Rasch, S. Hu, and L. Mitas, Density dependence of fixed-node errors in diffusion quantum Monte Carlo: Triplet pair correlations, Chem. Phys. Lett. **591**, 170 (2014).

[9] K. M. Rasch, S. Hu, and L. Mitas, Fixed-node errors in quantum Monte Carlo: Interplay of electron density and node nonlinearities, J. Chem. Phys. **140**, 041102 (2014).

[10] J. B. Anderson, Quantum chemistry by random walk, J. Chem. Phys. **65**, 4121 (1976).

[11] S. Zhang and M. H. Kalos, Exact Monte Carlo calculation for few-electron systems, Phys. Rev. Lett. **67**, 3074 (1991).

[12] J. W. Moskowitz, K. E. Schmidt, and M. H. Kalos, A new look at correlation energy in atomic and molecular systems. II. the application of the Green's function Monte Carlo method to LiH, J. Chem. Phys. **77**, 349 (1982).

[13] L. K. Wagner, M. Bajdich, and L. Mitas, QWalk: A quantum Monte Carlo program for electronic structure, J. Comput. Phys. **228**, 3390 (2009).

[14] R. J. White and F. H. Stillinger, Electron correlation in three-electron atoms and ions, Phys. Rev. A **3**, 1521 (1971).

[15] D. Bressanini, D. M. Ceperley, and P. J. Reynolds, *What Do We Know about Wave Function Nodes?* (World Scientific, Singapore, 2002), Chap. 1.

[16] Z.-C. Yan, M. Tambasco, and G. W. F. Drake, Energies and oscillator strengths for lithiumlike ions, Phys. Rev. A **57**, 1652 (1998).
[17] H. Ågren, J. Olsen, H. J. Aa. Jensen, and P. Jørgensen, Accurate static and dynamic polarizabilities of Li^-, Phys. Rev. A **40**, 2265 (1989).
[18] H. Tatewaki and T. Koga, Contracted Gaussian type basis functions revisited, J. Chem. Phys. **104**, 8493 (1996).
[19] F. W. King, Progress on high precision calculations for the ground state of atomic lithium, J. Molecul. Struc.: TheoChem **400**, 7 (1996).
[20] G. Haeffler, D. Hanstorp, I. Kiyan, A. E. Klinkmuller, U. Ljungblad, and D. J. Pegg, Electron affinity of Li: A state-selective measurement, Phys. Rev. A **53**, 4127 (1996).
[21] C. F. Fischer, Convergence studies of MCHF calculations for Be and Li^-, J. Phys. B **26**, 855 (1993).
[22] C. Filippi and C. J. Umrigar, Multiconfiguration wavefunctions for quantum Monte Carlo calculations of first-row diatomic molecules, J. Chem. Phys. **105**, 213 (1996).
[23] D. Bressanini, G. Morosi, and S. Tarasco, An investigation of nodal structures and the construction of trial wave functions, J. Chem. Phys. **123**, 204109 (2005).
[24] A. K. Ray, J. L. Fry, and C. W. Myles, A configuration interaction study of small lithium clusters, J. Phys. B **18**, 381 (1985).
[25] I. Boustani, W. Pewestorf, P. Fantucci, V. Bonacic-Koutecky, and J. Koutecky, Systematic *ab initio* configuration-interaction study of alkali-metal clusters: Relation between electronic structure and geometry of small Li clusters, Phys. Rev. B **35**, 9437 (1987).
[26] R. O. Jones, A. I. Lichtenstein, and J. Hutter, Density functional study of structure and bonding in lithium clusteres Li_n and their oxides Li_nO, J. Chem. Phys. **106**, 4566 (1997).
[27] R. Rousseau and D. Marx, *Ab initio* calculations on small lithium clusters, Phys. Rev. A **56**, 617 (1997).
[28] S. E. Wheeler, K. W. Sattelmeyer, P. v. R. Schleyer, and H. F. Schaefer, Binding energies of small lithium clusters (Li_n) and hydrogenated lithium clusters (Li_nH), J. Chem. Phys. **120**, 4683 (2004).
[29] D. Nissenbaum, L. Spanu, C. Attaccalite, B. Barbiellini, and A. Bansil, The resonating-valence-bond ground state of Li nanoclusters, Phys. Rev. B **79**, 035416 (2009).
[30] R. Rousseau and D. Marx, Exploring the electronic structure of elemental lithium: From small molecules to nanoclusters, bulk metal, and surfaces, Chem. Eur. J. **6**, 2982 (2000).
[31] M. Verdicchio, S. Evangelisti, T. Leininger, and A. Monari, On the triplet ground state of tetrahedral X_4 clusters (X = Li, Na, K, Cu), J. Chem. Phys. **136**, 094301 (2012).
[32] M. E. Alikhani and S. Shaik, A topological study of the ferromagnetic "no-pair bonding" in maximum-spin lithium clusters: $^{n+1}Li_n (n = 2-6)$, Theor. Chem. Acc. **116**, 390 (2006).
[33] V. Bonacic-Koutecky, J. Gaus, M. F. Guest, L. Cespiva, and J. Koutecky, *Ab initio* Ci study of the electronic structure and geometry of neutral and cationic hydrogenated lithium clusters, Chem. Phys. Lett. **206**, 528 (1993).
[34] R. K. Owen, Ph.D. thesis, Quantum Monte Carlo methods and lithium clusters' properties, University of California, Berkeley, 1990.
[35] B. K. Rao and P. Jena, Physics of small metal clusters: Topology, magnetism, and electronic structure, Phys. Rev. B **32**, 2058 (1985).
[36] C. H. Wu, Experimental investigation of a stable lithium cluster. The thermochemical study of the molecule Li_4, J. Phys. Chem. **87**, 1534 (1983).
[37] C. Brechignac, H. Busch, P. Cahuzac, and J. Leygnier, Dissociation pathways and binding energies of lithium clusters from evaporation experiments, J. Chem. Phys. **101**, 6992 (1994).
[38] G. Sugiyama, G. Zerah, and B. J. Alder, Ground-state properties of metallic lithium, Physica A **156**, 144 (1989).
[39] H. Eckstein and W. Schattke, Variational quantum Monte Carlo ground state of lithium on a slater orbital basis, Physica A **216**, 151 (1995).
[40] G. Yao, J. G. Xu, and X. W. Wang, Pseudopotential variational quantum Monte Carlo approach to bcc lithium, Phys. Rev. B **54**, 8393 (1996).
[41] C. Filippi and D. M. Ceperley, Quantum Monte Carlo calculation of compton profiles of solid lithium, Phys. Rev. B **59**, 7907 (1999).
[42] M. Hanfland, K. Syassen, N. E. Christensen, and D. L. Novikov, New high-pressure phases of lithium, Nature (London) **408**, 174 (2000).
[43] S. Deemyad and J. S. Schilling, Superconducting phase diagram of Li metal in nearly hydrostatic pressures up to 67 GPa, Phys. Rev. Lett. **91**, 167001 (2003).
[44] J. B. Neaton and N. W. Ashcroft, Pairing in dense lithium, Nature (London) **400**, 141 (1999).
[45] C. J. Pickard and R. J. Needs, Dense low-coordination phases of lithium, Phys. Rev. Lett. **102**, 146401 (2009).
[46] F. Herbstein and B. Averbach, The structure of lithium-magnesium solid solutions—I: Measurements on the bragg reflections, Acta Metall. **4**, 407 (1956).
[47] W. Pearson, *Handbook of Lattice Spacings and Structures of Metals* (Pergamon, New York, 1958).
[48] M. R. Nadler and C. P. Kempier, Crystallographic data 186. Lithium, Anal. Chem. **31**, 2109 (1959).
[49] S. H. Kellington, D. Loveridge, and J. M. Titman, The lattice parameters of some alloys of lithium, Br. J. Appl. Phys. **2**, 1162 (1969).
[50] S. N. Vaidya, I. C. Getting, and G. C. Kennedy, The compression of the alkali metals to 45 kbar, J. Phys. Chem. Solids **32**, 2545 (1971).
[51] M. S. Anderson and C. A. Swenson, Experimental equations of state for cesium and lithium metals to 20 kbar and the high-pressure behavior of the alkali metals, Phys. Rev. B **31**, 668 (1985).
[52] R. Gaudoin and W. M. C. Foulkes, *Ab initio* calculations of bulk moduli and comparison with experiment, Phys. Rev. B **66**, 052104 (2002).
[53] J. Kolorenc and L. Mitas, Quantum Monte Carlo calculations of structural properties of FeO under pressure, Phys. Rev. Lett. **101**, 185502 (2008).
[54] J. Kolorenc, S. Hu, and L. Mitas, Wave functions for quantum Monte Carlo calculations in solids: Orbitals from density functional theory with hybrid exchange-correlation functionals, Phys. Rev. B **82**, 115108 (2010).
[55] C. Lin, F. H. Zong, and D. M. Ceperley, Twist-averaged boundary conditions in continuum quantum Monte Carlo algorithms, Phys. Rev. E **64**, 016702 (2001).

[56] S. Chiesa, D. M. Ceperley, R. M. Martin, and M. Holzmann, Finite-size error in many-body simulations with long-range interactions, Phys. Rev. Lett. **97**, 076404 (2006).

[57] D. Bohm and D. Pines, A collective description of electron interactions: III. coulomb interactions in a degenerate electron gas, Phys. Rev. **92**, 609 (1953).

[58] M. Bajdich, L. Mitas, G. Drobny, L. K. Wagner, and K. E. Schmidt, Pfaffian pairing wave functions in electronic-structure quantum Monte Carlo simulations, Phys. Rev. Lett. **96**, 130201 (2006).

[59] M. Bajdich, L. Mitas, L. K. Wagner, and K. E. Schmidt, Pfaffian pairing and backflow wavefunctions for electronic structure quantum Monte Carlo methods, Phys. Rev. B **77**, 115112 (2008).

[60] P. Staikov, A. Kara, and T. S. Rahman, First-principles studies of the thermodynamic properties of bulk Li, J. Phys.: Condens. Matter **9**, 2135 (1997).

[61] K. A. J. Gschneidner, Physical properties and interrelationships of metallic and semimetallic elements, Solid State Phys. **16**, 275 (1964).

[62] W. T. Hicks, Evaluation of vapor pressure data for mercury, lithium, sodium, and potassium, J. Chem. Phys. **38**, 1873 (1963).

[63] I. G. Gurtubay, R. Gaudoin, and J. M. Pitarke, Benchmark quantum Monte Carlo calculations of the ground-state kinetic, interaction and total energy of the three-dimensional electron gas, J. Phys.: Condens. Matter **22**, 065501 (2010).

[64] P. López Ríos, A. Ma, N. D. Drummond, M. D. Towler, and R. J. Needs, Inhomogeneous backflow transformations in quantum Monte Carlo calculations, Phys. Rev. E **74**, 066701 (2006).

[65] Y. Kwon, D. M. Ceperley, and R. M. Martin, Effects of backflow correlation in the three-dimensional electron gas: Quantum Monte Carlo study, Phys. Rev. B **58**, 6800 (1998).

[66] M. Holzmann, D. M. Ceperley, C. Pierleoni, and K. Esler, Backflow correlations for the electron gas and metallic hydrogen, Phys. Rev. E **68**, 046707 (2003).